Journal of Environmental Chemical Engineering 14 (2026) 121977

Contents lists available at ScienceDirect

Journal of Environmental Chemical Engineering

journal homepage: www.elsevier.com/locate/jece

Recovery of Cerium(III) from aqueous solutions via selective adsorption using a three-layer bio-based composite

Bendhiba Badredine Berfai [a], Rima Hamel [a], Mihaela Cibian [b,c,*], Éric Loranger [a,d], Bruno Chabot [a,d]

[a] Institut d'innovations en écomatériaux, écoproduits et écoénergies, Université du Québec à Trois-Rivières, 3351 boul. des Forges, Trois-Rivières, (Québec) G8Z 4M3, Canada
[b] Département de biochimie, chimie, physique et science forensique, Université du Québec à Trois-Rivières, 3351 boul. des Forges, Trois-Rivières ,(Québec) G8Z 4M3, Canada
[c] Institut de recherche sur l'hydrogène, Université du Québec à Trois-Rivières, 3351 boul. des Forges, C.P. 500, Trois-Rivières, (Québec) G9A 5H7, Canada
[d] Département de génie mécanique, Université du Québec à Trois-Rivières, 3351 boul. des Forges, Trois-Rivières, (Québec) G8Z 4M3, Canada

ARTICLE INFO

Keywords:
Cerium recovery
Chitosan
Phosphorylated cellulose
Bio-based composite sorbent
Adsorption
Circular economy

ABSTRACT

As the demand for critical rare earth elements increases, their recovery from e-waste has become a sustainable alternative to traditional mining. Cerium, widely used in strategic technologies, remains challenging to recover efficiently. In this study, a three-layer bio-based composite adsorbent containing cellulose, phosphorylated cellulose, and electrospun chitosan nanofibers was developed to selectively adsorb and recover Ce^{3+} ions from aqueous solutions. The composite's constituents strongly influenced its adsorption performance: phosphorylated cellulose introduced phosphate groups that enhanced Ce^{3+} binding through electrostatic interactions, while chitosan nanofibers provided amino and hydroxyl sites that improved chelation, porosity, and mechanical integrity. The optimized combination of these components achieved a balance between functionality, permeability, and stability. Characterization (e.g., scanning electron microscopy, energy-dispersive X-ray spectroscopy, image analysis) confirmed the uniform distribution of active layers and the presence of functional groups responsible for adsorption. Batch adsorption tests revealed a high adsorption capacity of over 64 mg/g within 60 min, following a pseudo-first-order kinetic model and the Langmuir isotherm behavior. Thermodynamic analysis indicated an exothermic process, and the composite exhibited selectivity toward Ce^{3+} and Nd^{3+} over Cu^{2+}. Cerium was effectively desorbed and recovered, and the material maintained over 83% of its performance after four cycles, demonstrating its strong potential for sustainable rare earth recovery in line with circular economy principles.

1. Introduction

The rapid advancement of technology and the significant rise in the production of electronic products have led to a major environmental issue: the accumulation of electrical and electronic waste, commonly referred to as e-waste [1]. E-waste includes any faulty or obsolete electronic devices [2]. This type of waste, exhibiting alarming growth, presents a twofold challenge due to its concurrent hazardous nature and inherent value [3]. On the one hand, the increasing worldwide use of electronic devices is leading to a considerable rise in end-of-life byproducts [4], which presents a significant environmental threat and danger to human health [5,6]. Due to the presence of non-biodegradable heavy metals [7], these pollutants can contaminate air, soil, and water, with severe consequences for ecosystems and public health [8,9]. On the other hand, e-waste is considered valuable because it contains a wide variety of recyclable materials, such as plastics, glass, and metals, including rare earth elements (REEs) [10,11]. Therefore, the recovery of REEs from e-waste has emerged as a sustainable alternative to conventional mining, aligning with circular economy principles and the transition toward green technologies [12,13]. Today, countries such as Canada consider REEs to be essential, as they are critical to the energy transition [14–17]. In addition, the move towards a low-carbon

* Corresponding author at: Département de biochimie, chimie, physique et science forensique, Université du Québec à Trois-Rivières, 3351 boul. des Forges, Trois-Rivières, (Québec) G8Z 4M3, Canada.
E-mail address: mihaela.cibian@uqtr.ca (M. Cibian).

https://doi.org/10.1016/j.jece.2026.121977
Received 16 September 2025; Received in revised form 28 January 2026; Accepted 25 February 2026
Available online 26 February 2026

economy, the fight against climate change, and the adoption of low greenhouse gas emission technologies will increase demand for essential and strategic minerals [18,19]. This interconnection between e-waste, critical metals, and sustainable resource management highlights the necessity of developing environmentally friendly recovery routes for REEs [20,21]. The complex relationship between e-waste, greenhouse gas emissions, energy transition, and critical metals underlines the importance of sustainable management and efficient recovery of REEs from secondary resources.

The recovery of REEs plays a key role in promoting a circular economy [22,23]. However, conventional methods, such as hydrometallurgical and pyrometallurgical processes, are often costly, energy-intensive, and generate toxic waste [24–28]. Due to its great abundance, strategic significance, and extensive application [29], cerium (Ce) stands out among REEs [30]. It is widely used from catalysis, glass polishing, and fuel cells, to electronic devices [31]. Thus, it is also among the most abundant rare earth elements in electronic waste [32]. Its redox couple (Ce^{3+}/Ce^{4+}) endow it with unique reactivity and catalytic properties, making it indispensable for several industrial sectors [33,34]. It is also a common component in many everyday devices such as smartphones, flat-screen TVs, optical lenses, and LED lights [29, 35]. Considering these factors, cerium was selected as the target element for our work, which aims to evaluate sustainable adsorbent materials and develop an environmentally friendly recovery process that supports greener recycling technologies for REEs. Cerium is present in the Earth's upper crust at about 64 ppm [35], and occurs mainly as trivalent (Ce^{3+}) and tetravalent (Ce^{4+}) ions. Its redox reactions are essential for catalytic applications [36], with high demand in different industrial sectors [37]. For example, cerium is frequently used in petroleum refining processes, such as fluid catalytic cracking [38], and in vehicle catalytic converters to reduce harmful emissions [39]. Primary sources of cerium include monazite and bastnäsite, while secondary sources comprise phosphogypsum, red mud, NiMH batteries, and spent catalysts [31]. Extracting cerium from secondary sources is becoming essential to enhance its availability and minimize the harm associated with improper waste disposal [38,39].

Several techniques have been developed for the extraction and separation of metal ions like cerium from aqueous solutions, including solvent extraction, ion exchange, adsorption, precipitation, membrane filtration, and electrochemical methods [40–45]. Due to its low cost, operational simplicity, and high efficiency at trace metal concentrations, adsorption has emerged as one of the most sustainable and selective techniques for REE recovery [46–49]. Adsorption is a proven method for capturing cerium in an aqueous environment [50–53]. Various investigations have been carried out to develop an adsorbent material for extracting metals from aqueous solutions [54,55]. Still, they have faced challenges such as high production costs, elevated energy consumption, by-product generation, and the difficulty of regenerating adsorbents for long-term reuse [56–58]. Thus, it is essential to direct research efforts toward creating adsorbent materials that will overcome these limitations [59].

Overall, our work aims to contribute to the development of efficient, eco-friendly sorbents for REE recovery from aqueous solutions, in line with circular economy strategies and sustainable material innovation. We recently developed a new three-layer bio-based composite sorbent formed of cellulose, phosphorylated cellulose, and electrospun nanofibrous chitosan, which can maintain its structural integrity in an aqueous environment [60]. This configuration integrates electrospun chitosan nanofibers as the outer layers and phosphorylated cellulose as the core, forming a stable and permeable structure that ensures high accessibility of active sites. The material demonstrated potential for removing Cerium(III) from aqueous solutions. However, further studies are needed to better understand the role of each component in the composite's adsorption capacity and its impact on the accessibility of adsorption sites.

Thus, the primary goal herein is to incorporate phosphate and amino functional groups at an optimized ratio in the bio-based composite material, for tailoring its property of adsorbing Cerium(III) from water solutions, while preserving its permeability and access to these active sites. Adsorption selectivity has also been studied to determine the potential capacity of the three-layer bio-based sorbent to recover Cerium (III) from a mixture of several rare-earth elements. Compared to other studies, our approach focuses on a three-layer composite system combining cellulose, phosphorylated cellulose, and chitosan nanofibers, which provides a more complex architecture and enhanced functional diversity. This configuration allows the simultaneous contribution of electrostatic interactions and chelation sites, offering higher selectivity for cerium ions and faster kinetics.

2. Materials and methods

2.1. Materials

Low molecular weight chitosan (CS, deacetylation degree 75–85%) from Sigma-Aldrich and polyethylene oxide (PEO, $M_n \approx 900{,}000\ g{\cdot}mol^{-1}$) from Sigma-Aldrich were used to prepare the electrospinning solutions. Chitosan was dissolved in concentrated acetic acid (99.7%, ACS reagent grade, Fisher Scientific) and blended with PEO to facilitate the electrospinning of the polymer mixture. Cerium(III) nitrate hexahydrate ($Ce(NO_3)_3{\cdot}6H_2O \geq 99.5\%$, Sigma-Aldrich) was used as the target element for Ce^{3+} ion adsorption experiments. Copper (II) sulfate pentahydrate ($CuSO_4{\cdot}5H_2O \geq 99\%$, Sigma-Aldrich) and neodymium(III) chloride hexahydrate ($NdCl_3{\cdot}6H_2O$) were used in competitive adsorption tests to evaluate selectivity. Six aqueous eluent solutions were selected for desorption studies based on literature data: ethylenediaminetetraacetic acid (EDTA) 0.05 M, hydrochloric acid (HCl) 0.01 M, sodium hydroxide (NaOH) 0.1 M, sodium chloride (NaCl) 1.0 M, a mixture of EDTA and NaOH, and a mixture of EDTA and HCl solutions. All reagents were of analytical grade and used without further purification. Aqueous solutions were prepared using deionized water. Bleached hardwood kraft pulp (BHKP), labeled KP, was supplied by Kruger Inc. (Trois-Rivières, Canada) and was used to prepare phosphorylated pulp, labeled PKP.

2.2. Methods

2.2.1. Preparation of the three-layer bio-based composite adsorbent

The bio-based composite adsorbent was prepared according to the procedure outlined in our previous publication [60]. First, bleached hardwood kraft pulp fibers (KP) were phosphorylated using the method described by Shi and colleagues [61], which involved the use of phosphoric acid and phosphate esters in molten urea. The fibers were then washed with deionized water and an HCl solution 0.1 N to ensure the protonation of the phosphate groups. The washed fibers were then dried, yielding phosphorylated kraft pulp (PKP). Handsheets (60 g/m^2 basis weight) containing mixtures of KP and PKP fibers (ratios 100:0, 80:20, and 60:40) were prepared using the TAPPI T 205 sp-18 standard method. Most of the samples used in this study were made from a cellulosic handsheet with a KP:PKP ratio of 60:40, which was used to produce the central core of the three-layer bio-based composite adsorbent materials. A chitosan-polyethylene oxide (CS-PEO) solution was prepared by dissolving chitosan in acetic acid (90% w/v) and polyethylene oxide in water (1.5% w/v). Both solutions were mixed at a 4:3 mass ratio and stirred for 2 h. Then, the CS-PEO solution was electrospun onto both sides of a piece of the KP:PKP handsheet under specific voltage, flow rate, and distance from the syringe to the collector surface, as previously described [60]. The electrospinning time, ranging from 75 to 210 min, was varied to study the influence of the electrospun coating weight on the composite's performance. The resulting composite material was finally dried overnight in a conditioning room at 23 °C and 50% of relative humidity (TAPPI Standard No. 402-sp-03).

2.2.2. Characterization of the three-layer bio-based composite adsorbents

Various analytical technologies were used to thoroughly examine representative samples of each composite material. A Hitachi SU1510 X-ray scanning electron microscope (SEM), equipped with an Oxford energy-dispersive X-ray spectroscopy (EDX) detector, was used to examine the surface morphology of the materials and analyze their elemental composition. The average fiber diameter was measured using ImageJ software (National Institutes of Health, USA), based on 100 individual measurements per sample. All characterizations and measurements were repeated at least three times to ensure the quality and reliability of the results.

The phosphorus content of the KP:PKP handsheet was determined at three different ratios: 0% (KP:PKP ratio of 100:0), 2.5% (KP:PKP ratio of 80:20), and 5% (KP:PKP ratio of 60:40), using inductively coupled plasma optical emission spectrometry (ICP-OES, Agilent 5100, Agilent Technologies, Santa Clara, CA, USA). The phosphorus content is expressed as wt% (weight percent). Phosphate standard solutions (0.3–60 mg/L) were first prepared from monobasic potassium phosphate (KH_2PO_4) and allowed to equilibrate for 24 h. These solutions were used to generate a calibration curve for the ICP-OES spectrometer. Then, handsheet samples (0.5 g of KP:PKP) were mixed with 10 mL of a solution of concentrated sulfuric acid and 10 mL of hydrogen peroxide (H_2SO_4/H_2O_2), followed by thermal digestion. The resulting solutions were then diluted to 100 mL in a volumetric flask. This treatment converted phosphorus into phosphate, which was subsequently measured by ICP-OES. The total surface charge density of the materials was determined by conductimetric titration.

To study and optimize the effects of electrospun chitosan nanofibers coat weight and amino functional group content of the bio-based composite material, the impacts of electrospinning time on pore size and water flux through the bio-based composite were assessed using a dead-end stainless-steel cell (HP4750 from Sterlitech, USA) with an active membrane area of 14.6 cm^2. The composite samples used for the tests had a KP:PKP ratio of 60:40. The electrospinning time was varied from 0 to 210 min, labeled M0min, M75min, M120min, M165min, and M210min. Before testing, the bio-based composite samples were pre-compacted with distilled water at 5 psi for 10 min to achieve steady water flux and ensure that all pores are open. Permeation tests were conducted at a pressure of 7 psi and room temperature, using 0.1 L of deionized water. The water flux was calculated using Eq. (1) [62]:

$$J = \frac{V}{A \times t} \tag{1}$$

where J is the water flux (L/m^2 h), V is the filtrate volume (L), A is the surface area of the bio-based composite (m^2), and t is the filtration time (h).

To determine the diameter of the largest pores in the material, the Young-Laplace Eq. (2) [62] was used:

$$d = \frac{4\gamma \cos\theta}{P} \tag{2}$$

where P represents the bubble point pressure (MPa), γ is the surface tension at the air–liquid interface (N/m), θ is the liquid-solid contact angle, which is assumed to be 0° when a gas bubble penetrates a pore of equivalent diameter, and d is the average diameter of the largest pore (μm).

The surface charge of the composite was evaluated by determining the point of zero charge (PZC) by measuring the zeta potential (ζ) as a function of pH, following the methods described in [63]. The suspensions' ionic strength was maintained constant using a 1 mM NaCl solution. To ensure proper dispersion, the samples were sonicated after adjusting the pH from 2 to 11 with 0.1 M HCl and NaOH solutions. The zeta potential of the suspensions was measured at room temperature using a Zetasizer Nano ZS instrument (Malvern Panalytical). The pH at which the zero potential axis intersects the ζ = f(pH) curve was identified as the PZC. This analysis provides insight into the surface charge behavior of the material across different pH levels, which is essential for predicting the adsorption performance toward metals such as Ce^{3+}.

2.2.3. Adsorption experiments

A stock solution of Cerium(III) at 100 mg/L was prepared by dissolving cerium nitrate hexahydrate (0.0312 g) in deionized water and then diluting to 100 mL with deionized water in a volumetric flask. To investigate the ability of the adsorbent media in removing cerium from water, a series of tests were conducted using 50 mL samples of solution initially containing 100 mg/L of cerium. Samples of 50 mg of the three-layer bio-based composite adsorbent at a KP:PKP ratio of 60:40 were used for all experiments. Tests were conducted at 25 °C and pH 6.8, with continuous stirring at 150 rpm using an orbital shaker (ORBIT Environ shaker, Lab-Line). The concentration of residual cerium in the aqueous solution was measured using ICP-OES. The maximum cerium adsorption capacity of the sorbent media was calculated using Eq. (3).

$$q_t = \frac{C_0V_0 - \sum_{1}^{i-1} C_iV - C_i[V_0 - (i-1)V]}{m} \tag{3}$$

where:

q_t: Amount of cerium ion adsorbed at time t (mg/g);
C_0: Initial cerium ion concentration (mg/L);
C_i: Cerium ion concentration at time t (mg/L);
V_0: Initial volume of solution (L);
V: Volume of the solution sample at time t (L);
m: Mass of the sorbent (g).

2.2.3.1. Adsorption kinetics. The adsorption kinetics of cerium ions by the three-layer bio-based composite adsorbent was studied by placing 50 mg of the media into 50 mL of a solution at an initial concentration of cerium (C_0) of 100 mg/L. Tests were conducted at 25 °C and pH 6.8, with continuous stirring at 150 rpm. The adsorption trials were conducted over a period of 0–180 min, with samples collected at 0, 5, 10, 15, 30, 60, 120, and 180 min. The concentration of cerium was determined using ICP-OES. Non-linear pseudo first-order (Eq. 4) and non-linear pseudo second-order (Eq. 5) models were used to fit the experimental data:

$$q_t = q_e(1 - \exp^{-k_1 t}) \tag{4}$$

$$q_t = \frac{k_2 q_e^2 t}{1 + k_2 q_e t} \tag{5}$$

where:

q_e: Amount of cerium ion adsorbed at equilibrium (mg/g);
q_t: Amount of cerium ion adsorbed (mg/g) at time t (min);
k_1: Pseudo first order adsorption rate constant (min^{-1});
k_2: Pseudo second order adsorption rate constant (g/(g min)).

2.2.3.2. Thermodynamic analysis. During adsorption, thermodynamics plays an important role. Thermodynamic parameters: Gibbs free energy values (ΔG°), enthalpy change (ΔH°), and entropy change (ΔS°) determine the degree of spontaneity of the process and its feasibility. These parameters were determined by Eqs. (6) and (7), respectively.

$$\Delta G^\circ = -RT \ln k_c \tag{6}$$

$$\Delta G^\circ = \Delta H^\circ - T\Delta S^\circ \tag{7}$$

where R is the universal gas constant (8.314 J/mol K), T is the temperature (K) and k_c is the adsorption equilibrium constant. The latter is calculating using (Eq. 8).

$$k_c = \frac{C_s}{C_e} = \frac{(C_0 - C_e)}{C_e} \quad (8)$$

where C_s and C_e are the equilibrium concentrations of Cerium(III) on the adsorbent material and in the aqueous solution in (mg/L); C_0 is the initial cerium ion concentration in the aqueous solution (mg/L). The relationship between the equilibrium constant (k_c) and the temperature is given by the van't Hoff equation (Eq. 9).

$$\ln k_c = -\frac{\Delta H^\circ}{RT} + \frac{\Delta S^\circ}{R} \quad (9)$$

The enthalpy and entropy changes are obtained from the slope $\Delta H^\circ/R$ and the intercept $\Delta S^\circ/R$ by plotting ln k_c versus $1/T$ according to Eq. (9). Negative values of ΔG° indicate that adsorption is a spontaneous and favorable process, where no energy input from outside the system is required. Negative values of ΔH° suggest the exothermic nature of the adsorption process, while positive values indicate an endothermic nature. Negative ΔS° values evidence that randomness decreases at the solid-solution interface during adsorption, while positive ΔS° values indicate the opposite.

2.2.3.3. Equilibrium isotherms. The sorption isotherms were studied under batch conditions at 25 °C, 45 °C, and 60 °C for initial cerium concentrations ranging from 50 to 300 mg/L. After 120 min contact time, samples of 2 mL were taken from the flasks, and cerium concentrations were determined by ICP-OES. The Langmuir (Eq. 14) and the Freundlich (Eq. 11) equations were used to fit the experimental data:

$$q_e = \frac{q_m K_L C_e}{1 + K_L C_e} \quad (10)$$

where:

q_m: Maximum adsorption capacity (mg/g);
K_L: Langmuir constant (L/mg);
q_e: Amount of cerium ion adsorbed at equilibrium (mg/g);
C_e: Cerium ion concentration at equilibrium (mg/L)
and

$$q_e = K_F C_e^{1/n} \quad (11)$$

where:

n: Adsorption intensity constant;
K_F: Freundlich constant (mg/g);
q_e: Amount of cerium ion adsorbed at equilibrium (mg/g);
C_e: Cerium ion concentration at equilibrium (mg/L).

2.2.3.4. Selective adsorption. Multicomponent aqueous solutions containing Ce^{3+}, Nd^{3+}, and Cu^{2+} ions were used to evaluate the composite material's selectivity toward some critical and strategic metals. By combining equal amounts (33.33 mg/L) of each metal ion in a volume of 50 mL, a total metal ion concentration of 100 mg/L was achieved. Equimolar conditions are thus achieved for Ce^{3+} and Nd^{3+} ions, while the molar concentration of Cu^{2+} ions is 2.2 times higher vs those of rear earth metal ions. The adsorbent (50 mg) was added, and the solution was agitated (150 rpm) at a pH of 6.8 for 3 h at room temperature to ensure adsorption equilibrium, taking into account the difference in molar masses of each ion to ensure equimolar conditions. After the adsorption process, ICP-OES was employed to detect the residual concentrations of Ce^{3+}, Nd^{3+}, and Cu^{2+}. The selectivity coefficient (K-REE) was calculated to quantify the preference for Ce^{3+} over competing ions. First, Eq. 12 was used to calculate the adsorption capacity of each metal ion at equilibrium:

$$q_e = \frac{(C_0 - C_e) \times V}{m} \quad (12)$$

where:

q_e: Amount of ion adsorbed at equilibrium (mg/g);
C_0: Initial ion concentration (mg/L);
C_e: Ion concentration at equilibrium (mg/L);
V: Volume of solution (L);
m: Mass of the sorbent (mg).

Then, the selectivity coefficients K_{REE} were calculated to quantify the selectivity of the adsorbent for rare earth elements (REE) over other metal ions using Eq. 13 [64]:

$$K_{REE} = \frac{q_{e,REE}}{q_{e,M}} \quad (13)$$

where $q_{e,REE}$, and $q_{e,M}$ are the adsorption capacities of the rare earth element and the competing metal ion, respectively.

2.2.4. Desorption and regeneration studies

The investigation focused on recovering cerium ions and evaluating the desorption efficiency and reusability of the three-layer bio-based composite adsorbent through multiple sorption-desorption cycles. After the adsorption phase, the sorbent samples were immersed in various eluent solutions, including EDTA (0.05 M), HCl (0.01 M), NaOH (0.1 M), NaCl (1 M), EDTA/NaOH (80:20), and EDTA/HCl (80:20), and allowed to desorb for 24 h at room temperature while being stirred continuously. Prior to reuse, the sorbent materials were dried at 40 °C for 12 h following desorption and were thoroughly rinsed with deionized water to eliminate any residual eluent. Adsorption and desorption cycles were then conducted up to four times. ICP-OES was used to measure the adsorption capacity of the regenerated adsorbent at the end of each cycle. Desorption efficiency and adsorption capacity were calculated after each cycle, confirming that a gradual decrease beyond four cycles may be attributed to minor structural degradation or loss of active sites. The desorption efficiency was calculated using Eq. 14 [64]:

$$DE = \frac{C \times V}{q \times m} \times 100\% \quad (14)$$

where:

C: concentration of adsorbates in the desorption solution (mg/L);
q: The amount of adsorbate adsorbed on the material before the desorption experiment (mg/g);
V: Volume of solution (L);
m: Mass of the sorbent (mg).

2.2.5. Recovery of cerium

After desorption using an EDTA (0.05 M)/HCl (0.1 M) eluent mixture (80:20), cerium was recovered as Ce^{4+}-EDTA complexes in the aqueous phase. The eluate was concentrated by evaporation at 70 °C under continuous stirring. To induce cerium decomplexation and precipitation as cerium hydroxide, the pH was gradually raised to 10 by adding aliquots of a 1 M NaOH solution, under vigorous agitation. Then, the suspension was aged for 12 h at room temperature to ensure complete precipitation. The resulting solid was separated by vacuum filtration using a 0.45 μm membrane filter, thoroughly washed with deionized water to remove residual impurities, and dried at 80 °C for 12 h. Finally, the dried material was calcined in a laboratory muffle furnace at 400 °C for 4 h to eliminate organic residues and convert the hydroxide into cerium dioxide (CeO_2). A colorimetric confirmation using Arsenazo III reagent verified the oxidation of Ce^{3+} to Ce^{4+} during desorption. This step serves as a qualitative indicator of oxidation in acidic media.

3. Results and discussion

3.1. Characterization of the three-layer bio-based composite adsorbent

The structure of the three-layer bio-based composite has been investigated using SEM and EDX analyses. Fig. 1 presents SEM

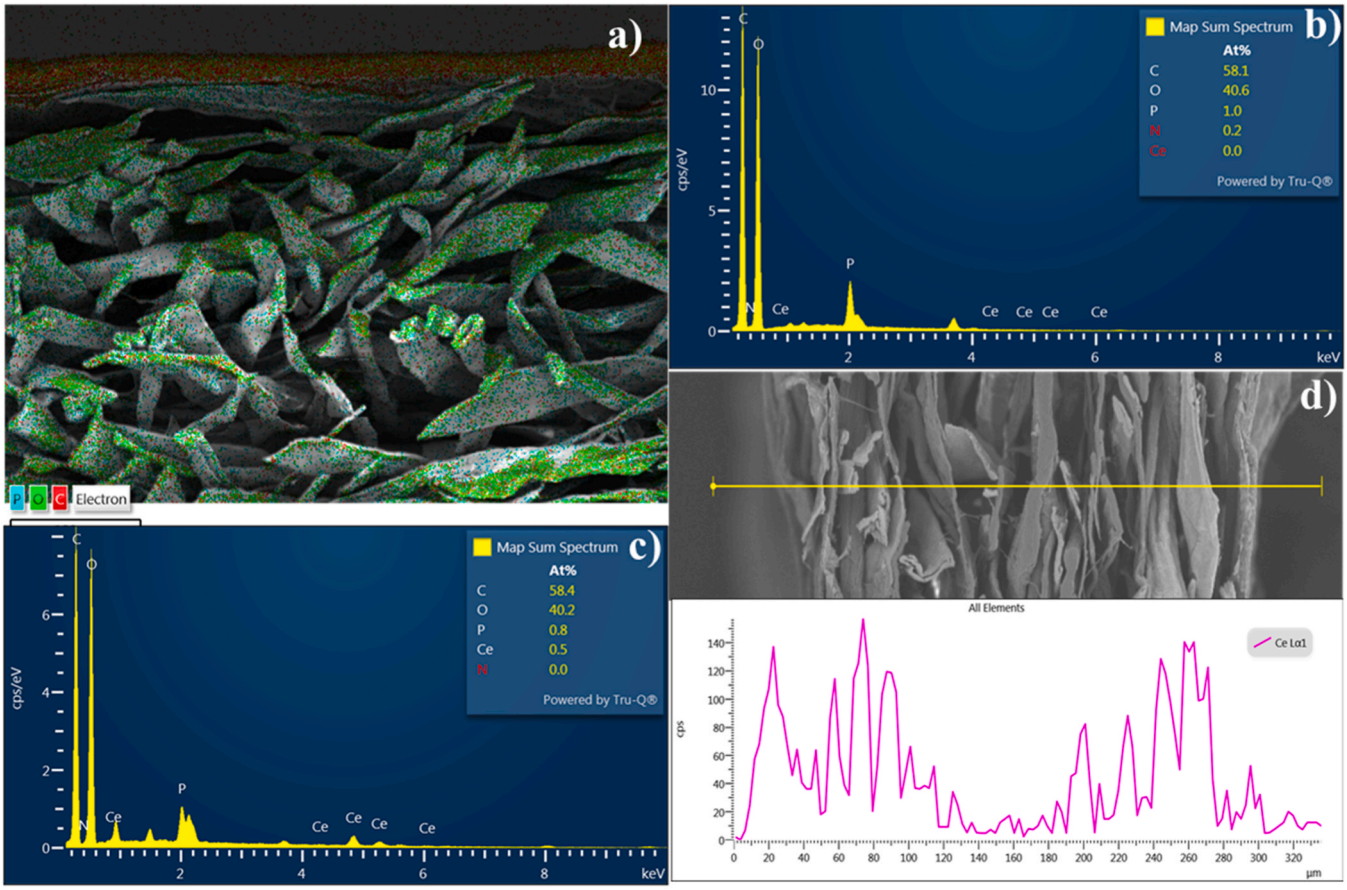

Fig. 1. SEM micrographs and EDX elemental mapping of representative bio-based composite samples with a KP:PKP ratio of 60:40: a) SEM of the cross-section of the bio-based composite, b) EDX mapping of the composite before adsorption, c) EDX mapping of the composite after adsorption, d) SEM imaging combined with EDX scanning analysis of the cross-section after adsorption.

micrographs and EDX elemental mapping of a typical bio-based composite material sample (core cellulose handsheet (KP:PKP of ratio 60:40) with electrospun chitosan coating). Fig. 1a clearly illustrates two distinct layers. The bottom layer shows a blue coloration, indicating the presence of phosphorus, which confirms the presence of phosphorylated cellulose in the KP:PKP handsheet. This observation is consistent with the proposed sandwich structure, where the central core layer is composed of phosphorylated cellulose. Conversely, the top layer shows no phosphorus, suggesting it mainly comprises chitosan from the electrospun nanofibers deposited on the central core cellulose handsheet. In the EDX mapping of the composite before adsorption (Fig. 1b), as expected, no signal corresponding to cerium is present, while in the EDX mapping of the composite after adsorption (Fig. 1c), the cerium peak is identified. Fig. 1d shows the SEM imaging, combined with EDX scanning analysis, revealing a non-uniform distribution of cerium on the composite's layers.

The intensity profile of the Ce Lα₁ signal (Fig. 1d) indicates a preference for cerium accumulation at the surface and edges of the composite material (where chitosan is prevalent), while the inner regions (cellulose and phosphorylated cellulose-rich) exhibit a lower density of cerium. This distribution could arise from restricted diffusion of Ce^{3+} ions in the deeper layers, attributed to porosity limitations and the significant volume of hydrated cerium complexes. Moreover, this cerium distribution pattern could also result from instantaneous, surface-dominant adsorption, caused by the presence of more easily accessible functional groups (such as amines) in the chitosan thin layer electrospun on both sides of the central core cellulosic handsheet, or potentially by the saturation of surface-active sites, which hinders access to internal zones. These results suggest that continuous adsorption may be more advantageous than batch adsorption for future work.

Fig. 2a and Fig. 2b show a representative analysis of the chitosan nanofibers electrospun on top of the KP:PKP handsheet. An average nanofiber diameter of approximately 114.34 ± 17.17 nm was determined (Fig. 2a). As shown in Fig. 2b, the nanofibers appear uniform, continuous, and evenly distributed. The small diameter of the fibers contributes to a high surface-to-volume ratio, resulting in a high surface area. This exposes more amino groups (–NH_2) from chitosan on the surface of the composite, thereby enhancing the material's adsorption capacity for metals, including cerium.

3.2. *Effect of phosphorus content on total surface charge density of the three-layer bio-based composite adsorbent*

Increasing the phosphorus content in the sorbent material by varying the ratio of KP to PKP fibers in the pulp mixture introduces negatively charged phosphate groups onto the fiber surfaces, thereby providing additional adsorption sites for Ce^{3+} ions [60]. Phosphorus content determination for each pulp mixture resulted in phosphorus content of 0% (ratio KP:PKP of 100:0), 2.5% (ratio KP:PKP of 80:20), and 5% (ratio KP:PKP of 60:40), respectively. The total surface charge was measured for three handsheet samples with varying phosphorus levels (Table 1).

The phosphorus-free sample (0%) exhibited a minimal total charge, reflecting the limited presence of acidic functional groups, primarily carboxyl groups. In contrast, samples with higher phosphorus content showed a significant increase in surface charge density. This trend was especially noticeable in samples with 2.5% and 5% phosphorus, where the total charge reached 1895 ± 79 mmol/kg and 1960 ± 138 mmol/kg, respectively. This increase in negative surface charge, resulting from

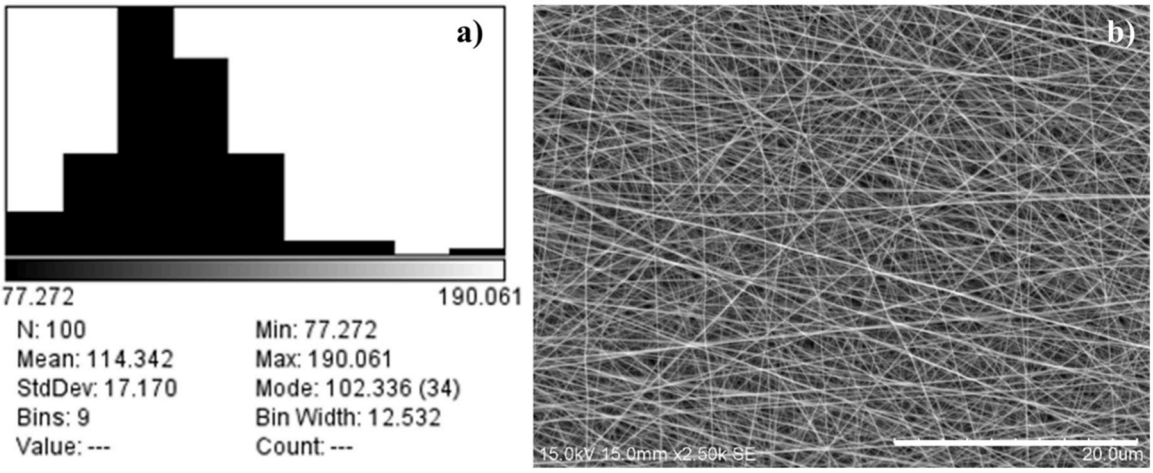

Fig. 2. a) Average diameter of the chitosan nanofibers electrospun onto the KP:PKP handsheet (ratio 60:40), b) SEM image of the top surface of the three-layer bio-based composite adsorbent.

Table 1
Total surface charge density and phosphorus content of handsheet samples at various KP:PKP ratios

Sample	KP:PKP (100:0)	KP:PKP (80:20)	KP:PKP (60:40)
Phosphorus content(wt%)	0	2.5	5
Total charge* (mmol/kg)	182 ± 76	1895 ± 79	1960 ± 138

*Standard deviations are calculated based on three measurements per sample.

the addition of phosphate groups, is expected to provide additional adsorption sites and enhance the material's overall ability to adsorb cerium ions through electrostatic interactions.

3.3. Effect of electrospinning time on the three-layer bio-based composite pore size and permeability

Table 2 presents the effect of electrospinning time on the overall permeability of the three-layer bio-based composite adsorbent (KP:PKP of 60:40).

Results indicate a significant reduction in water flux, along with a decrease in mean pore size, as the electrospinning time increases from 0 to 210 min. This trend suggests that the reduction is due to the higher coat weight of chitosan nanofibers deposited on the KP:PKP central core handsheet. Thus, partial obstruction of the interfiber pores is likely to be caused, resulting in a decrease in water flux and a reduction in mean pore size. Therefore, the amount of chitosan nanofibers applied to both sides of the cellulosic handsheet has a significant influence on the overall porosity of the composite. To optimize the balance between electrospinning time and the reduction of mean pore size and water flux, an electrospinning duration of 75 min was chosen for the adsorption experiments. At this electrospinning duration, the mean pore size and the water flux obtained for the composite were 7.7 ± 0.5 μm and 150.48 ± 2.19 $Lm^{-2}h^{-1}$, respectively (Table 2).

Table 2
Effect of electrospinning time on mean pore size and water flux

Samples	Mean pore size (μm)	Water flux ($Lm^{-2}h^{-1}$)
M0min	20.75 ± 1.57	412.89 ± 1.28
M75min	7.7 ± 0.5	150.48 ± 2.19
M120min	5.05 ± 0.17	37.42 ± 1.72
M165min	1.95 ± 0.07	6.32 ± 0.88
M210min	1.58 ± 0.05	1.33 ± 0.16

3.4. Zeta potential

The pH of the solution plays a crucial role in the adsorption of heavy metals, as it directly affects both the metal ion speciation in solution and the surface charge characteristics of the adsorbent [65]. To characterize the surface charge of the composite and determine its point of zero charge (PZC), the variation of the zeta potential as a function of pH has been studied. Fig. 3 shows a positive charge at acidic pH (ζ = +21.7 mV at pH 2), resulting from the protonation of chitosan's amine groups ($–NH_3^+$). As pH increases, the zeta potential gradually decreases, and around pH 4.03 (the material's isoelectric point (IEP)), it reverses charge. Beyond this point, the surface acquires a negative charge, reaching ζ = -36.5 mV at pH 11 due to the combined effects of amine deprotonation and phosphate ionization in phosphorylated cellulose. This change shows that the composite's charge level strongly depends on the pH of the aqueous environment. Therefore, the optimal pH range for the adsorption of Ce^{3+} by the composite is between 4 and 7, where the surface is sufficiently negatively charged, and the cerium mainly exists in the Ce^{3+} form [66]. A previous study [60] demonstrated that pH 6.8 provides the optimal adsorption performance; therefore, this work was conducted exclusively under this condition.

3.5. Adsorption study

3.5.1. Effect of electrospinning time and phosphate content on adsorption capacity

This section examines the combined effect of the phosphorylation level of kraft fibers and the addition of a chitosan nanofiber layer, applied via electrospinning, on the composite material's capacity to adsorb Ce(III) ions. Fig. 4 shows how the adsorption capacity at equilibrium (q_e) changes with the concentration of phosphate groups in the absence of electrospinning treatment and when electrospinning treatment is applied..

The reference material, a handsheet sample made entirely of untreated kraft fibers (0% degree of phosphorylation) without electrospun chitosan nanofibers, shows a limited adsorption capacity of 7.49 mg/g, suggesting a lack of functional groups that can form specific interactions with Ce^{3+} ions. To better understand the effect of phosphorylation on kraft fibers, handsheets containing mixtures of untreated and phosphorylated kraft fibers at KP:PKP ratios of 80:20 (which corresponds to a 2.5% degree of phosphorylation of the untreated kraft pulp) and 60:40 (which corresponds to a 5% degree of phosphorylation of the untreated kraft pulp) were tested. The higher the degree of phosphorylation, the

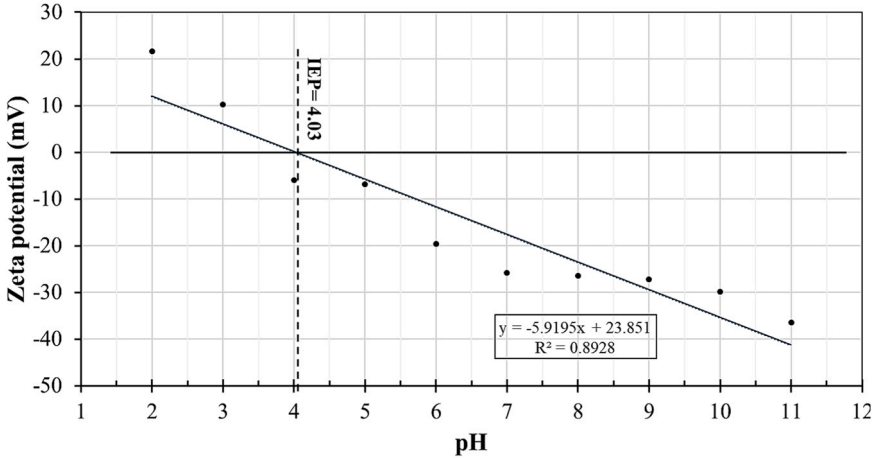

Fig. 3. Effect of pH on the zeta-potential of the three-layer bio-based composite and determination of the point of zero charge (PZC), the material's isoelectric point (IEP).

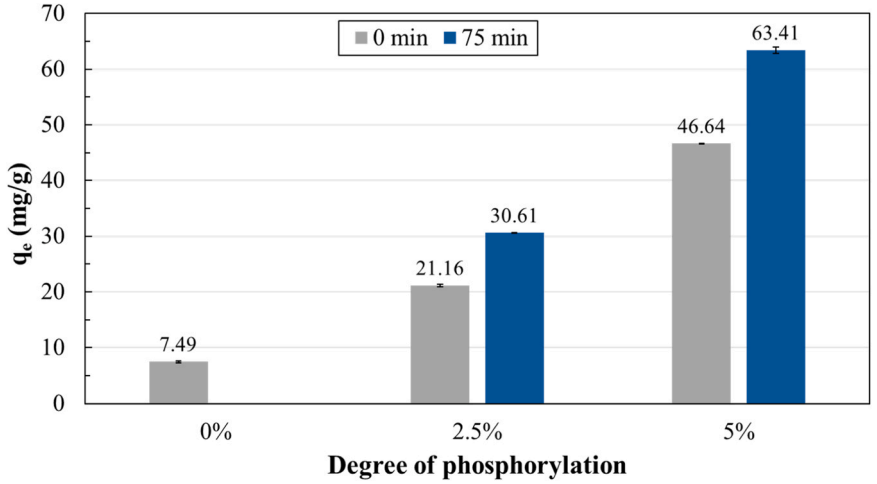

Fig. 4. Effect of electrospinning and phosphorylation on the adsorption capacity of the three-layer bio-based composite samples with phosphorus content of 0% (KP:PKP ratio of 100:0), 2.5% (80:20), 2.5% (80:20) + 75 min of chitosan electrospinning, 5% (60:40), and 5% (60:40) + 75 min of chitosan electrospinning. (C_0 = 100 mg/L, adsorbent mass = 50 mg, temperature = 25 °C, pH = 6.8, contact time = 60 min.).

higher the adsorption capacity. This enhancement is attributed to the introduction of phosphate groups, which provide specific electrostatic binding sites with Ce(III) ions [64]. To study the combined effects of phosphate and amino functional groups within the bio-based composite sorbent, electrospinning was performed for 75 min. Chitosan nanofibers were thus applied to both sides of the handsheet samples with KP:PKP ratios of 2.5% and 5% phosphorylated fibers. The 75-minute electrospinning duration was selected based on prior characterization data, which indicates that it provides the optimal balance between permeability and accessibility of active areas. Longer electrospinning times have shown an opposing effect, associated with increased densification of the fiber network, which reduces porosity and limits species movement to reactive sites (Section 3.3). The combination of various types of functional groups has a synergistic effect on the adsorption capacity of Ce(III) by the bio-based composite sorbent. On one hand, electrospun chitosan nanofibers introduce primary amines that interact favorably with anions or contribute to chelate metal cations [67]. Additionally, the hydroxyl groups in chitosan's structure contribute to adsorption, improving the material's overall effectiveness [68]. On the other hand, phosphorylation increases the density of phosphate-charged groups within the cellulosic support, promoting electrostatic interactions with these ions. Consequently, the integration of chemical and nanofiber structures has yielded a dual-functionalized system that proves to be highly effective for the adsorption of Ce(III) ions.

Furthermore, considering that the adsorption experiments were carried out at a pH of 6.8, these conditions favored Ce(III) chemistry, as indicated by speciation diagrams showing that Ce^{3+} remains the predominant species at this pH, with no significant formation of hydrolyzed or precipitated species such as $Ce(OH)_{3(s)}$ [66]. The combination of these approaches enables the development of a multifunctional composite material that ensures effective adsorption of rare earth elements.

3.5.2. *Adsorption kinetics*

Batch adsorption tests were carried out with an initial cerium ion concentration of 100 mg/L. Tests were conducted at 25°C and pH 6.8 using three-layer bio-based composite samples with a KP:PKP ratio of 60:40. Fig. 5 shows that the adsorption capacity of the three-layer bio-based composite adsorbent reaches an equilibrium within about 60 min of contact time. Therefore, this is the optimal choice for cerium adsorption experiments. To investigate the mechanisms involved in adsorption, nonlinear pseudo first-order and pseudo second-order kinetic model fittings of experimental data were studied and are shown in Fig. 5. Table 3 summarizes the fitting parameters of both models. Results indicate that the pseudo first-order kinetic model better describes the experimental data with a coefficient of determination (R^2) of 0.99. Since the sorbent material has functional groups that promote both

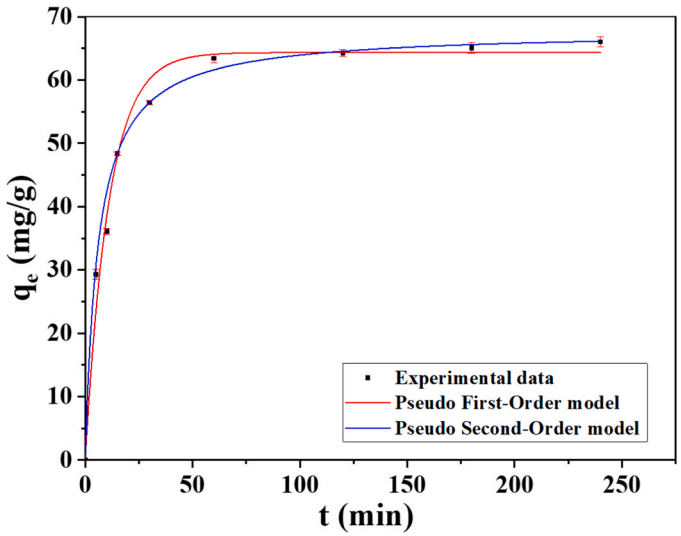

Fig. 5. Fitting of experimental data to adsorption kinetics pseudo first- and pseudo second-order models. Tests were conducted using three-layer bio-based composite samples with a KP:PKP ratio of 60:40. (C_0 = 100 mg/L, adsorbent mass = 50 mg, temperature = 25 °C, pH = 6.8, contact time = 60 min.).

Table 3
Summary of kinetic model parameters for cerium ion adsorption onto the three-layer bio-based composite sample with a KP:PKP ratio of 60:40

Pseudo first-order model				Pseudo second-order model		
q_{exp} (mg/g)	R^2	k_1 (min^{-1})	q_{eq} (mg/g)	R^2	k_2 (g/g min)	q_{eq} (mg/g)
64.26	0.99	0.091	64.35	0.95	0.002	67.79

electrostatic interactions (e.g., phosphate groups in phosphorylated cellulose) and chelation (e.g., amine groups in chitosan nanofibers), the overall adsorption rate is mainly governed by a physisorption mechanism rather than surface chemical reactions and should be regarded as the most plausible model for this study. This is consistent with the rapid initial uptake observed and the strong correlation between predicted and experimental capacities. Similar conclusions have been reported in studies where composites containing cellulose or chitosan exhibited a better fit with the pseudo first-order model [68], particularly when ionic interactions dominate the adsorption process. This conclusion is also in line with the strong electrostatic character of the interactions in cerium ion complexation, even in chelating environments, induced by the presence of electrons in the lanthanide core-type *f* orbitals (a characteristic of lanthanide complex formation) [69].

3.5.3. Adsorption isotherms

The adsorption isotherm evaluates the material's surface properties and adsorption capacity [70]. Figs. 6a and 6b present the Langmuir and Freundlich isotherm nonlinear fitting models of the experimental data. Experiments were conducted at 25 °C, 45 °C, and 60 °C at a pH of 6.8, with initial cerium concentrations varying from 50 to 300 mg/L. A three-layer bio-based composite sample with a KP:PKP ratio of 60:40 was used. The equilibrium time was set at 120 min based on the kinetic tests conducted previously. Table 4 summarizes the isotherm parameters obtained from nonlinear fitting models. The results indicate that, generally, the Langmuir model better describes the experimental data, exhibiting higher correlation coefficients (R^2) compared to the Freundlich isotherm, at most temperatures. These results suggest that Ce (III) adsorption onto the three-layer bio-based composite primarily occurs in a monolayer. The exothermic nature of the process is further supported by the observed decrease in the Langmuir constant K_L with increasing temperature [71]. Moreover, the Freundlich constant n was greater than 1 at all tested temperatures, confirming that the adsorption process was favorable.

3.5.4. Thermodynamic analysis

Thermodynamic analysis was carried out to assess the spontaneity and energetic nature of the adsorption process on the composite material studied, made up of cellulose, phosphorylated cellulose and chitosan nanofibers. The equilibrium constants k_c, determined at different temperatures (25 °C, 45 °C, and 60 °C), were used to calculate the standard thermodynamic parameters (Gibbs free energy change (ΔG°), enthalpy change (ΔH°), andentropy change (ΔS°)), according to the van't Hoff equation.

Based on the findings in Table 5, the negative Gibbs free energy change (ΔG°) (−1.45 kJ/mol at 25 °C) indicates that the adsorption is

Table 4
Summary of isotherm parameters for cerium ion adsorption onto the three-layer bio-based composite sample with a KP:PKP ratio of 60:40

	Freundlich			Langmuir		
T (°C)	K_F (mg/g)	n	R^2	q_{max} (mg/g)	K_L (L/mg)	R^2
25	4.903	1.848	0.98	134.63	0.009	0.99
45	5.303	2.430	0.96	62.38	0.014	0.95
60	1.506	1.757	0.94	65.86	0.005	0.97

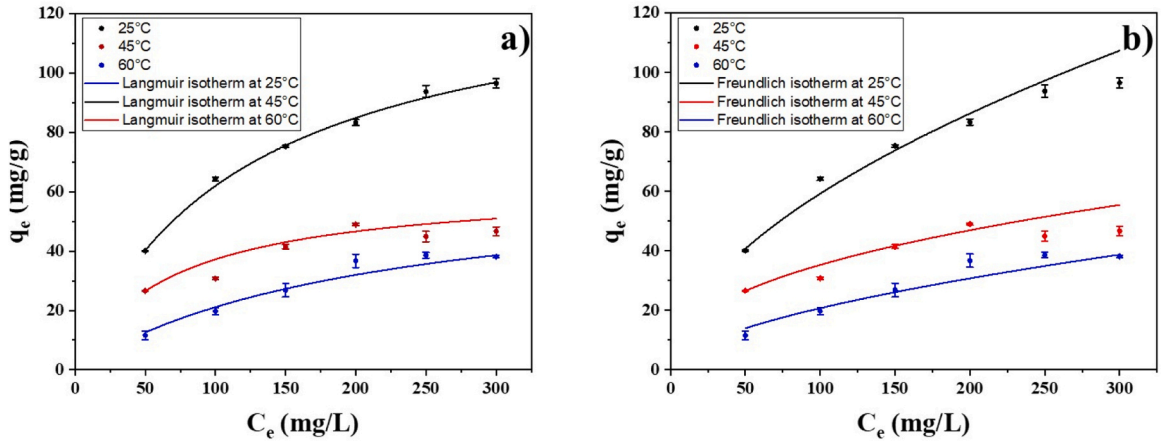

Fig. 6. Non-linear fitting of experimental data: a) Langmuir isotherm model, b) Freundlich isotherm models at 25 °C, 45 °C, and 60 °C. Tests were conducted using three-layer bio-based composite samples with a KP:PKP ratio of 60:40. (C_0 = 50–300 mg/L, adsorbent mass = 50 mg, pH = 6.8, contact time = 120 min.).

Table 5
Parameters of thermodynamic analysis

Temperature (°C)	q_e (mg/g)	C_e (mg/L)	$k_c = q_e/C_e$	ln (k_c)	ΔG° (kJ/mol)	ΔH° (kJ/mol)	ΔS° (J/mol·K)
25	64.26	35.74	1.79	0.59	-1.45	-47.60	-155.23
45	30.75	69.25	0.44	-0.81	+2.15		
60	19.72	80.28	0.25	-1.40	+3.89		

spontaneous at room temperature. However, as the temperature increases, ΔG° becomes less negative and eventually positive, reaching +2.15 kJ/mol at 45 °C and +3.89 at 60 °C. This progression clearly reflects a decline in spontaneity with rising temperature. The transition to positive ΔG° at higher temperatures reveals that the adsorption becomes thermodynamically unfavorable, which is consistent with the phenomenon of thermal desorption often observed in exothermic systems. The calculated standard enthalpy changes ΔH°= -47.60 kJ/mol supports this observation by showing that the adsorption is exothermic (heat is released during the process). Despite being moderate, this value is typical of physisorption (weak interactions (e.g., hydrogen bonds, electrostatic interactions, or van der Waals forces)involved) versus chemisorption. Furthermore, the standard entropy change (ΔS°) was found to be −155.23 J/mol·K, suggesting a decrease in randomness at the solid–liquid interface during the adsorption process. This entropy reduction reflects the formation of a more ordered system, likely due to the immobilization of Ce(III) ions on the adsorbent surface. The observed loss of configurational freedom can be attributed to strong adsorbent–adsorbate interactions and the structured rearrangement of water molecules around the active functional groups, such as phosphate and amine moieties. Such a negative entropy change is not uncommon in adsorption systems where specific interactions constrain the mobility of adsorbed species, resulting in a more rigid interfacial configuration. The observed thermodynamic behavior can be linked to the complex surface chemistry and structure of the phosphorylated cellulose–chitosan bio-based adsorbent. More specifically, the presence of various functional groups such as phosphate, hydroxyl, and amine likely contributes to the formation of multiple adsorption sites with varied affinities, resulting in temperature-sensitive interactions.

3.5.5. Comparative analysis of Cerium(III) removal effectiveness with various materials

Table 6 presents a comparative analysis of various sorbent materials for the removal of Cerium(III). At a pH of 6.8, the three-layer bio-based composite adsorbent (KP:PKP ratio of 60:40) shows a significant cerium adsorption capacity of 64.26 mg/g within 60 min. Activated carbon, commonly used as a conventional adsorbent, shows much lower performance under similar or even more favorable conditions. Activated carbon derived from rice straw reached only 4.13 mg/g after 500 min at pH 4, while that obtained from date seeds showed a moderate capacity of 24.58 mg/g at pH 5.7, with a contact time of 180 min. Compared to our composite, these values show lower adsorption capacity, while requiring significantly longer equilibrium times. Other materials, such as the amidoxime-modified biochar and the FeO_4–pectin–chitosan nanocomposite show lower adsorption capacities of 45.20 mg/g and 9.72 mg/g, respectively, under more acidic conditions and/or longer equilibrium times. These comparisons demonstrate that our three-layer bio-based composite adsorbs cerium ions more effectively, positioning it as a potentially good candidate for wastewater treatment and the recycling of electronic waste.

Table 6
Comparative analysis of adsorption capacity of various sorbent materials

Adsorbent Material	Maximum Adsorption Capacity (q_{max}) mg/g	Experimental Conditions	Ref.
Amidoxime-modified biochar	45.20	pH 6, 25 °C, equilibrium time: 100 min	[72]
Fe_3O_4–pectin–chitosan nanocomposite	9.72	pH 5, 25 °C, equilibrium time: 30 min	[73]
Activated carbon from rice straw	4.13	pH 4, 35 °C, equilibrium time: 500 min	[74]
Activated carbon derived from date seeds	24.58	pH 5.7, 25 °C, equilibrium time: 180 min	[75]
Hydrous ferric oxide (HFO)	Not specified	pH 4–10, 30–60 °C, equilibrium time: 60 min	[76]
Cellulose-phosphorylated cellulose/chitosan nanofiber composite	64.26	pH 6.8, 25 °C, equilibrium time: 60 min	This study

3.5.6. Selectivity of the three-layer bio-based composite adsorbent in the presence of other metallic ions

Ion selectivity is a crucial parameter that determines the material's ability to specifically recognize and capture target metal ions in the presence of competing species [77]. The selectivity of the three-layer bio-based composite adsorbent made of chitosan, cellulose, and phosphorylated cellulose toward cerium ions (Ce^{3+}) was also examined. Adsorption experiments were conducted in multicomponent aqueous solutions simultaneously containing Ce^{3+}, Nd^{3+}, and Cu^{2+} ions. Table 7 indicates that the bio-based composite has a strong affinity for trivalent rare earth metal ions. For Ce^{3+}, an adsorption capacity of 28.13 mg/g was achieved in the multicomponent system. In the same mixed system, neodymium (Nd^{3+}) displays a higher adsorption level of 30.23 mg/g, while copper (Cu^{2+}), being a divalent ion, is significantly less adsorbed at 19.18 mg/g. Selectivity coefficients, calculated as the ratio of the adsorption capacity of the rare earth metal ions to that of Cu^{2+}, were 1.47 and 1.58 for Ce^{3+} and Nd^{3+}, respectively (Table 7). These values indicate preferential adsorption of trivalent rare earth ions over divalent copper ions. This selective behavior can be attributed to several physicochemical factors. The phosphorylated functional groups on cellulose and the amine functionalities on chitosan serve as strong chelating agents [60], facilitating the formation of stable complexes with trivalent ions. Furthermore, the higher ionic charge and larger ionic radius of lanthanides enhance both electrostatic attractions and coordination interactions with the composite's active sites [69]. In summary, the three-layer bio-based composite adsorbent exhibits notable selectivity for trivalent rare earth metal ions (Nd^{3+} and Ce^{3+}) over divalent metal ions such as Cu^{2+}. This selectivity profile confirms the material's potential for separating rare earth elements from complex matrices, such as those found in electronic waste leachates, offering a promising solution for recovering critical metals in sustainable recycling strategies.

Table 7
Summary of selectivity tests for cerium vs. other metals on a three-layer bio-based composite sample with a KP:PKP ratio of 60:40

Ions	Adsorption capacity in a multicomponent solution (mg/g)	REE Selectivity vs Cu^{2+}	Selectivity comparison
Ce^{3+}	28.13	1.47	$Nd^{3+} > Ce^{3+} > Cu^{2+}$
Nd^{3+}	30.23	1.58	
Cu^{2+}	19.18	1	

3.6. Regeneration and reusability of the three-layer bio-based composite adsorbent

3.6.1. Desorption and concentration of cerium

Desorption of cerium ions from the three-layer composite material (KP:PKP ratio of 60:40) was carried out using six different eluents. Fig. 7a shows the desorption rate for each eluent and the change in weight of the adsorbent material. EDTA/HCl was the most effective eluant tested, with a desorption rate of 87% with minimal mass loss (3.34%). In comparison to EDTA and EDTA/NaOH, this result is due to a dual synergistic action: on one hand, HCl protonates the adsorption sites, promoting the release of Ce^{3+} ions, while on the other hand, EDTA forms stable complexes with the metal ions, facilitating their transfer into solution. At the end of the desorption step, the cerium initially present as Ce^{3+} is oxidized to Ce^{4+}. This was confirmed by a colorimetric assay using Arsenazo III reagent, known for its sensitivity to cerium oxidation states. In the presence of Ce^{4+}, the solution exhibits a characteristic purple color, clearly indicating the oxidation of trivalent cerium to its tetravalent form (Fig. 7b). This oxidation results from the oxidizing nature of the environment, especially due to the presence of HCl. This favors the conversion of Ce^{3+} to Ce^{4+}, a more stable species in an acidic and oxidizing medium [78]. The other eluent solutions evaluated for the desorption process yielded less satisfactory results. For example, NaOH and HCl alone resulted in high matrix degradation (mass losses of 25% and 20%, respectively), while EDTA/NaOH showed moderate yield with significant structural impact. EDTA, while gentle on the material, failed to yield adequate recovery results, achieving only 40%. Similarly, NaCl demonstrated limited effectiveness, attaining a recovery rate of 50%.

The EDTA/HCl system was the most effective desorption agent, facilitating the efficient and clean recovery of cerium ions, with the conversion of Ce^{3+} to Ce^{4+} in solution. After the desorption of cerium by the EDTA/HCl eluant mixture, the recovered cerium was transferred to an aqueous solution, as Ce^{4+}, for recycling. Concentration and precipitation steps were then carried out. The solution containing Ce^{4+}-EDTA was subjected to evaporation under stirring, then the pH was adjusted using NaOH to destabilize the complex and precipitate the cerium as hydroxide. The solid was filtered, washed with deionized water, and dried at 80 °C. A final calcination step yielded high-purity cerium dioxide (CeO_2), a material of strategic interest for numerous applications (catalysis, optics, oxygen storage, etc [79,80].). This comprehensive approach not only demonstrates the effectiveness of the three-layer bio-based composite adsorbent for the selective capture of cerium, but also facilitates its direct recovery in a reusable form, addressing the current challenges of circularity and recycling of critical materials.

3.6.2. Adsorption-desorption cycle

The regenerative capacity of an adsorbent is an important factor in evaluating its practical applicability, particularly for large-scale, cost-effective operations. To assess the reusability of the three-layer bio-based composite adsorbent (KP:PKP ratio of 60:40), four consecutive adsorption-desorption cycles were performed using Ce^{3+} ions as the target species. Between each cycle, the composite samples were thoroughly rinsed with distilled water and dried to restore their active sites. Fig. 8 illustrates the progression of adsorption capacity over successive adsorption and desorption cycles.

The initial desorption efficiency was 93.34%, but after four successive cycles, it decreased slightly to 77.91%, corresponding to an 83% retention of the initial performance. This gradual decline suggests that the composite material maintains good regeneration capacity despite a slight loss of efficiency over successive cycles. This decrease is likely attributable to the degradation of the chitosan nanofiber layers. Indeed, the acidic desorption medium (EDTA/HCl) promotes protonation of the chitosan amino groups. This protonation, along with mechanical agitation and prolonged immersion, speeds up the material's structural degradation, causing a gradual loss of active sites and a decline in adsorption performance. Figure S1 shows FTIR spectra of the composite material after the first regeneration cycle. It is clear that the peak related to chitosan has been altered, but despite this fact, the material remains quite effective even after repeated use, highlighting the structural strength of the composite matrix and the chemical stability of the functional phosphate and amine groups. These findings confirm that the three-layer bio-based composite maintains durability over multiple uses.

4. Conclusions

A three-layer bio-based composite adsorbent was developed for the selective recovery of Ce(III) from aqueous media. The material was produced using an environmentally benign electrospinning technique, where a nanofibrous chitosan layer was applied to a 60:40 phosphorylated kraft pulp/kraft pulp core, forming a mechanically stable and chemically active core–shell structure. The composite exhibited a high adsorption capacity of 64 mg/g within 60 min, following a pseudo first-order kinetic model and a Langmuir isotherm, indicating monolayer adsorption on a homogeneous surface. It also showed strong selectivity toward Ce(III) and Nd(III) ions over Cu(II), highlighting its efficiency for rare-earth recovery. Morphological (SEM) and elemental (EDX) analyses confirmed the uniform electrospun layer and the incorporation of active sites. The composite retained 83% of its performance after four adsorption/desorption cycles, confirming its durability. Thermodynamic analysis revealed an exothermic and spontaneous process.

This work introduces an innovative multilayer bio-based structure

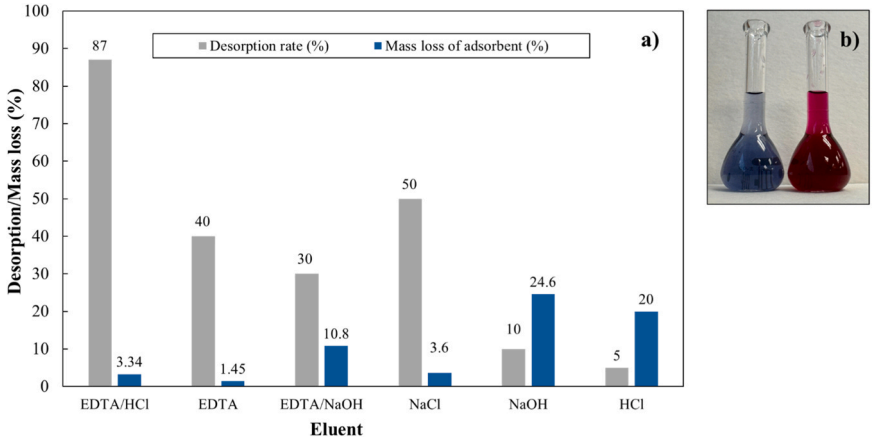

Fig. 7. a) Desorption efficiency of cerium ions and mass loss of the adsorbent using various eluents, b) Effect of cerium oxidation states on solution color developed by Arsenazo III reagent. Tests were conducted using three-layer bio-based composite samples with a KP:PKP ratio of 60:40.

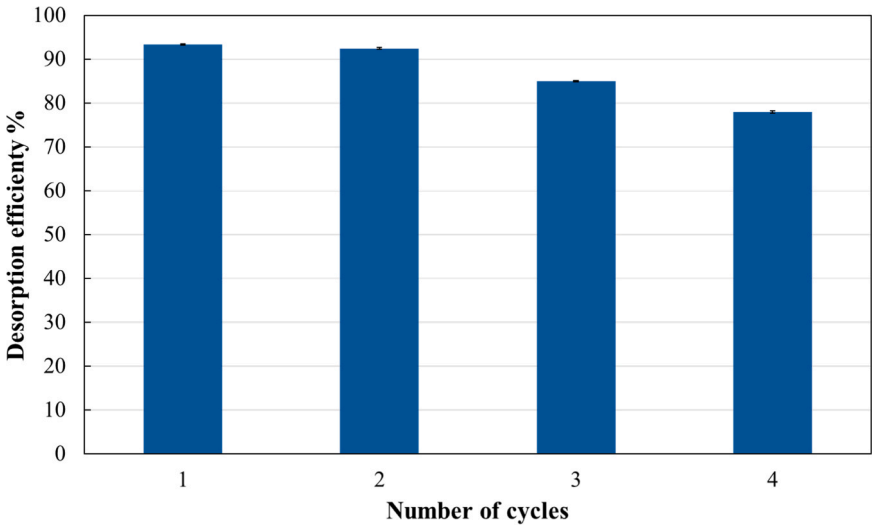

Fig. 8. Adsorption-desorption cycles of the three-layer bio-based composite adsorbent. Tests were conducted using three-layer bio-based composite samples with a KP:PKP ratio of 60:40.

combining phosphorylation and electrospinning, providing higher adsorption capacity and better reusability than previously reported cellulose- or chitosan-based adsorbents. Overall, the developed composite represents a sustainable and efficient solution for cerium recovery from secondary sources, supporting circular economy principles.

Declaration of Generative AI and AI-assisted technologies in the writing process

During the preparation of this work, the author(s) used [Grammarly, DeepL] in order to [improve the English language quality]. After using this tool/service, the author(s) reviewed and edited the content as needed and take full responsibility for the content of the published article.

CRediT authorship contribution statement

Mihaela Cibian: Writing – review & editing, Validation, Supervision, Resources, Funding acquisition. **Éric Loranger:** Writing – review & editing. **Bendhiba Badredine Berfai:** Writing – review & editing, Writing – original draft, Validation, Methodology, Investigation, Formal analysis, Conceptualization. **Rima Hamel:** Formal analysis. **Bruno Chabot:** Writing – review & editing, Validation, Supervision, Resources, Project administration, Methodology, Funding acquisition, Formal analysis, Conceptualization.

Declaration of Competing Interest

Hereby, the authors declare no competing interests.

Acknowledgments

The authors thank the Natural Sciences and Engineering Research Council of Canada (NSERC), grants no. RGPIN-2022–03510 and RGPIN-2020-6968, for financial support, and the University of Quebec à Trois-Rivières for providing space, materials, and equipment to complete this research.

Appendix A. Supporting information

Supplementary data associated with this article can be found in the online version at doi:10.1016/j.jece.2026.121977.

Data availability

Data will be made available on request.

References

[1] P. Thakur, S. Kumar, Evaluation of e-waste status, management strategies, and legislations, Int. J. Environ. Sci. Technol. 19 (7) (2022) 6957–6966.
[2] R. Moradi, M. Yazdi, A. Haghighi, A. Nedjati, Sustainable resilient E-waste management in London: a circular economy perspective, Heliyon 10 (13) (2024).
[3] V.N. Bhoi, T. Shah, E-waste: a new environmental challenge, Int. J. Adv. Res. Comput. Sci. Softw. Eng. 2 (4) (2014).
[4] B. Niu, E. Shanshan, Q. Song, Z. Xu, B. Han, Y. Qin, Physicochemical reactions in e-waste recycling, Nat. Rev. Chem. (2024) 1–18.
[5] S. Arya, S. Kumar, E-waste in India at a glance: current trends, regulations, challenges and management strategies, J. Clean. Prod. 271 (2020) 122707.
[6] P. Dias, A.M. Bernardes, N. Huda, e-waste management and practices in developed and developing countries, Electron. Waste. Recycl. Reprocess. a Sustain. Future (2022) 15–32.
[7] P. Kumar, S. Singh, A. Gacem, K.K. Yadav, J.K. Bhutto, M.A. Alreshidi, M. Kumar, A. Kumar, V.K. Yadav, S. Soni, A review on e-waste contamination, toxicity, and sustainable clean-up approaches for its management, Toxicology (2024) 153904.
[8] A. Kumar, P. Singh, M.K. Khanna, Sustainable E-Waste Management and Its Effect on Environment and Human Health. in Integrated Waste Management: A Sustainable Approach from Waste to Wealth, Springer, 2024, pp. 349–373.
[9] J. Bagum, S. Sahoo, A. Samanta, A. Nalluri, S.S. Sana, P. Bhardwaj, K. Ramesh, V. Raghavan, A.P. Garg, M. Choudhury, *Introduction to Environmental Waste: A Serious Issue*, in. Waste Management and Treatment, CRC Press, 2025, pp. 1–25.
[10] W. Yang, H.S. Lee, Y.-K. Park, J. Lee, Recovery of non-metallic useable materials from e-waste: A review, Chemosphere (2024) 141435.
[11] A. Bhattarai, R.L. Gardas, S.N. Yadav, S.K. Chatterjee, R.K. Dev, Recovery of rare earth elements (REEs) from different sources of E-waste and their potential applications, A Crit. Rev. (2024).
[12] A.I. Rasee, E. Awual, A.I. Rehan, M.S. Hossain, R. Waliullah, K.T. Kubra, M. C. Sheikh, M.S. Salman, M.N. Hasan, M.M. Hasan, Efficient separation, adsorption, and recovery of Samarium (III) ions using novel ligand-based composite adsorbent, Surf. Interfaces 41 (2023) 103276.
[13] M.R. Awual, T. Kobayashi, Y. Miyazaki, R. Motokawa, H. Shiwaku, S. Suzuki, Y. Okamoto, T. Yaita, Selective lanthanide sorption and mechanism using novel hybrid Lewis base (N-methyl-N-phenyl-1, 10-phenanthroline-2-carboxamide) ligand modified adsorbent, J. Hazard. Mater. 252 (2013) 313–320.
[14] Attílio, L.A., J.R. Faria and E. Silva, Critical Minerals, Electric Goods, and the Global Energy Transition. The University of Auckland Business School Research Paper Series, 2024.
[15] L. Depraiter, S. Goutte, The role and challenges of rare earths in the energy transition, Resour. Policy 86 (2023) 104137.
[16] S.-L. Liu, H.-R. Fan, X. Liu, J. Meng, A.R. Butcher, L. Yann, K.-F. Yang, X.-C. Li, Global rare earth elements projects: new developments and supply chains, Ore Geol. Rev. 157 (2023) 105428.
[17] A.B. Patil, R.P. Struis, C. Ludwig, Opportunities in critical rare earth metal recycling value chains for economic growth with sustainable technological innovations, Circ. Econ. Sustain. 3 (2) (2023) 1127–1140.
[18] D'Orazio, P. and G. Vasishtha, Critical Minerals and the Low-Carbon Transition: Economic Implications for Emerging Markets and Developing Economies.

[19] S. Dou, D. Xu, Y. Zhu, R. Keenan, Critical mineral sustainable supply: challenges and governance, Futures 146 (2023) 103101.
[20] M.R. Awual, T. Kobayashi, H. Shiwaku, Y. Miyazaki, R. Motokawa, S. Suzuki, Y. Okamoto, T. Yaita, Evaluation of lanthanide sorption and their coordination mechanism by EXAFS measurement using novel hybrid adsorbent, Chem. Eng. J. 225 (2013) 558–566.
[21] M.R. Awual, N.H. Alharthi, Y. Okamoto, M.R. Karim, M.E. Halim, M.M. Hasan, M. M. Rahman, M.M. Islam, M.A. Khaleque, M.C. Sheikh, Ligand field effect for Dysprosium (III) and Lutetium (III) adsorption and EXAFS coordination with novel composite nanomaterials, Chem. Eng. J. 320 (2017) 427–435.
[22] V. Balaram, Sustainable recovery of rare earth elements by recycling of E-waste for a circular economy: perspectives and recent advances, Environ. Mater. Waste (2024) 499–544.
[23] S.H. Gheewala, Material recycling in a circular economy—A systems view, Wiley Interdiscip. Rev. Energy Environ. 13 (1) (2024) e503.
[24] A. Saidi, R. El Khawaja, D.C. Boffito, A review of traditional and intensified hydrometallurgy techniques to remove chromium and vanadium from solid industrial waste, ACS Eng. Au 4 (1) (2023) 49–70.
[25] A.B. Botelho Junior, U.K. Sultana, J. Vaughan, Hydrometallurgical processing of E-waste and metal recovery, Manag. Electron. Waste. Resour. Recovery Technol. Regul. (2024) 234–288.
[26] P. Paranjape, M.D. Yadav, Recent advances in the approaches to recover rare earths and precious metals from E-waste: a mini-review, Can. J. Chem. Eng. 101 (2) (2023) 1043–1054.
[27] Z. Sun, H. Cao, Y. Xiao, J. Sietsma, W. Jin, H. Agterhuis, Y. Yang, Toward sustainability for recovery of critical metals from electronic waste: the hydrochemistry processes, ACS Sustain. Chem. & Eng. 5 (1) (2017) 21–40.
[28] R. Nithya, C. Sivasankari, A. Thirunavukkarasu, Electronic waste generation, regulation and metal recovery: a review, Environ. Chem. Lett. 19 (2021) 1347–1368.
[29] K. Kowsuki, R. Nirmala, Y.-H. Ra, R. Navamathavan, Recent advances in cerium oxide-based nanocomposites in synthesis, characterization, and energy storage applications: a comprehensive review, Results Chem. (5) (2023) 100877.
[30] J.T. Dahle, Y. Arai, Environmental geochemistry of cerium: applications and toxicology of cerium oxide nanoparticles, Int. J. Environ. Res. Public Health 12 (2) (2015) 1253–1278.
[31] M.R. Awual, M.M. Hasan, A. Shahat, M. Naushad, H. Shiwaku, T. Yaita, Investigation of ligand immobilized nano-composite adsorbent for efficient cerium (III) detection and recovery, Chem. Eng. J. 265 (2015) 210–218.
[32] A. Poulos, A. Poulos, E-Waste, Secret Life Chem. (2021) 181–187.
[33] M.R. Awual, T. Yaita, H. Shiwaku, Design a novel optical adsorbent for simultaneous ultra-trace cerium (III) detection, sorption and recovery, Chem. Eng. J. 228 (2013) 327–335.
[34] Q. Zhu, J. Xiao, C. Deng, H. Ding, T. Huang, G. Xu, L. Zhang, Cerium doping induces in-situ reconstruction of Ni5P4 to enhance urea-assisted water splitting, Electrochim. Acta (2025) 147556.
[35] E. Allahkarami, B. Rezai, Removal of cerium from different aqueous solutions using different adsorbents: A review, Process Saf. Environ. Prot. 124 (2019) 345–362.
[36] X. Tan, Y. Zhong, Z. Wang, Y. Geng, S. Xiao, Y. Zhang, J. Huang, Mapping cerium flows in China: A dynamic material flow analysis, Resour. Policy 99 (2024) 105386.
[37] Z.C. Sims, M.S. Kesler, H.B. Henderson, E. Castillo, T. Fishman, D. Weiss, P. Singleton, R. Eggert, S.K. McCall, O. Rios, How cerium and lanthanum as coproducts promote stable rare earth production and new alloys, J. Sustain. Metall. 8 (3) (2022) 1225–1234.
[38] A.B.V. de Farias, T.B. da Costa, M.G.C. da Silva, M.G.A. Vieira, Development of novel composite adsorbents based on biopolymers/vermiculite using the ionic imprinting technique for cerium biosorption, J. Environ. Chem. Eng. 10 (6) (2022) 108730.
[39] A. Shahbaz, A systematic review on leaching of rare earth metals from primary and secondary sources, Miner. Eng. 184 (2022) 107632.
[40] E. Allahkarami, B. Rezai, A literature review of cerium recovery from different aqueous solutions, J. Environ. Chem. Eng. 9 (1) (2021) 104956.
[41] M.R. Awual, M.N. Hasan, M.M. Hasan, M.S. Salman, M.C. Sheikh, K.T. Kubra, M. S. Islam, H.M. Marwani, A. Islam, M.A. Khaleque, Green and robust adsorption and recovery of Europium (III) with a mechanism using hybrid donor conjugate materials, Sep. Purif. Technol. 319 (2023) 124088.
[42] K.T. Kubra, M.M. Hasan, M.N. Hasan, M.S. Salman, M.A. Khaleque, M.C. Sheikh, A. I. Rehan, A.I. Rasee, R. Waliullah, M.E. Awual, The heavy lanthanide of Thulium (III) separation and recovery using specific ligand-based facial composite adsorbent, Colloids Surf. A Physicochem. Eng. Asp. 667 (2023) 131415.
[43] M.N. Hasan, M.S. Salman, M.M. Hasan, K.T. Kubra, M.C. Sheikh, A.I. Rehan, A. I. Rasee, M.E. Awual, R. Waliullah, M.S. Hossain, Assessing sustainable Lutetium (III) ions adsorption and recovery using novel composite hybrid nanomaterials, J. Mol. Struct. 1276 (2023) 134795.
[44] M.M. Hasan, K.T. Kubra, M.N. Hasan, M.E. Awual, M.S. Salman, M.C. Sheikh, A. I. Rehan, A.I. Rasee, R. Waliullah, M.S. Islam, Sustainable ligand-modified based composite material for the selective and effective cadmium (II) capturing from wastewater, J. Mol. Liq. 371 (2023) 121125.
[45] M.R. Awual, Efficient phosphate removal from water for controlling eutrophication using novel composite adsorbent, J. Clean. Prod. 228 (2019) 1311–1319.
[46] B. Ji, W. Zhang, Adsorption of cerium (III) by zeolites synthesized from kaolinite after rare earth elements (REEs) recovery, Chemosphere 303 (2022) 134941.
[47] K.T. Kubra, M.S. Salman, M.N. Hasan, A. Islam, S.H. Teo, M.M. Hasan, M.C. Sheikh, M.R. Awual, Sustainable detection and capturing of cerium (III) using ligand embedded solid-state conjugate adsorbent, J. Mol. Liq. 338 (2021) 116667.
[48] M.R. Awual, New type mesoporous conjugate material for selective optical copper (II) ions monitoring & removal from polluted waters, Chem. Eng. J. 307 (2017) 85–94.
[49] M.R. Awual, M.M. Hasan, A. Islam, A.M. Asiri, M.M. Rahman, Optimization of an innovative composited material for effective monitoring and removal of cobalt (II) from wastewater, J. Mol. Liq. 298 (2020) 112035.
[50] D.E. Al Momani, Z. Al Ansari, M. Ouda, M. Abujayyab, M. Kareem, T. Agbaje, B. Sizirici, Occurrence, treatment, and potential recovery of rare earth elements from wastewater in the context of a circular economy, J. Water Process Eng. 55 (2023) 104223.
[51] J. Bąk, P. Bulak, M. Kaczor, D. Kołodyńska, A. Bieganowski, Better Ce (III) Sorption Properties of Unprocessed Chitinous Waste from Hermetia illucens than Commercial Chitosans, Materials 17 (21) (2024) 5255.
[52] M.S. Salman, M.N. Hasan, M.M. Hasan, K.T. Kubra, M.C. Sheikh, A.I. Rehan, R. Waliullah, A.I. Rasee, M.E. Awual, M.S. Hossain, Improving copper (II) ion detection and adsorption from wastewater by the ligand-functionalized composite adsorbent, J. Mol. Struct. 1282 (2023) 135259.
[53] K.T. Kubra, M.S. Salman, H. Znad, M.N. Hasan, Efficient encapsulation of toxic dye from wastewater using biodegradable polymeric adsorbent, J. Mol. Liq. 329 (2021) 115541.
[54] A. Maftouh, O. El Fatni, S. El Hajjaji, M.W. Jawish, M. Sillanpää, Comp. Rev. Differ. Adsorpt. Tech. Use Heavy Met. Remov. Water Biointerface Res. Appl. Chem. 13 (2023) 397.
[55] M.M. Hasan, M.S. Salman, M.N. Hasan, A.I. Rehan, M.E. Awual, A.I. Rasee, R. Waliullah, M.S. Hossain, K.T. Kubra, M.C. Sheikh, Facial conjugate adsorbent for sustainable Pb (II) ion monitoring and removal from contaminated water, Colloids Surf. A Physicochem. Eng. Asp. 673 (2023) 131794.
[56] Z. Raji, A. Karim, A. Karam, S. Khalloufi, Adsorption of heavy metals: mechanisms, kinetics, and applications of various adsorbents in wastewater remediation—a review, Waste (2023) (MDPI).
[57] J. Chi, C. Wang, G. Zhou, X. Fu, X. Chen, X. Yin, Z. Zhang, Y. Wang, A critical review on separation and extraction of scandium from industrial wastes: Methods, difficulties, and mechanism, J. Environ. Chem. Eng. (2023) 111068.
[58] M.S. Salman, M.C. Sheikh, M.M. Hasan, M.N. Hasan, K.T. Kubra, A.I. Rehan, M. E. Awual, A.I. Rasee, R. Waliullah, M.S. Hossain, Chitosan-coated cotton fiber composite for efficient toxic dye encapsulation from aqueous media, Appl. Surf. Sci. 622 (2023) 157008.
[59] A.I. Rehan, A.I. Rasee, M.E. Awual, R. Waliullah, M.S. Hossain, K.T. Kubra, M. S. Salman, M.M. Hasan, M.N. Hasan, M.C. Sheikh, Improving toxic dye removal and remediation using novel nanocomposite fibrous adsorbent, Colloids Surf. A Physicochem. Eng. Asp. 673 (2023) 131859.
[60] B.B. Berfai, M. Cibian, B. Chabot, Development and structural characterization of a three-dimensional composite adsorbent material for Cerium (III) recovery from aqueous solution, Mater. Today Commun. 45 (2025) 112391.
[61] Y. Shi, D. Belosinschi, F. Brouillette, A. Belfkira, B. Chabot, Phosphorylation of Kraft fibers with phosphate esters, Carbohydr. Polym. 106 (2014) 121–127.
[62] I.I. Cárdenas Bates, É. Loranger, A.P. Mathew, B. Chabot, Cellulose reinforced electrospun chitosan nanofibers bio-based composite sorbent for water treatment applications, Cellulose 28 (8) (2021) 4865–4885.
[63] E.-H. Ablouh, F. Brouillette, M. Taourirte, H. Sehaqui, M. El Achaby, A. Belfkira, A highly efficient chemical approach to producing green phosphorylated cellulosic macromolecules, RSC Adv. 11 (39) (2021) 24206–24216.
[64] O. Pereao, K. Laatikainen, C. Bode-Aluko, I. Kochnev, O. Fatoba, A. Nechaev, L. Petrik, Adsorption of Ce3+ and Nd3+ by diglycolic acid functionalised electrospun polystyrene nanofiber from aqueous solution, Sep. Purif. Technol. 233 (2020) 116059.
[65] M.C. Sheikh, M.M. Hasan, M.N. Hasan, M.S. Salman, K.T. Kubra, M.E. Awual, R. Waliullah, A.I. Rasee, A.I. Rehan, M.S. Hossain, Toxic cadmium (II) monitoring and removal from aqueous solution using ligand-based facial composite adsorbent, J. Mol. Liq. 389 (2023) 122854.
[66] B. Bouchaud, J. Balmain, G. Bonnet, F. Pedraza, pH-distribution of cerium species in aqueous systems, J. Rare Earths 30 (6) (2012) 559–562.
[67] R. Waliullah, A.I. Rehan, M.E. Awual, A.I. Rasee, M.C. Sheikh, M.S. Salman, M. S. Hossain, M.M. Hasan, K.T. Kubra, M.N. Hasan, Optimization of toxic dye removal from contaminated water using chitosan-grafted novel nanocomposite adsorbent, J. Mol. Liq. 388 (2023) 122763.
[68] X. Chen, Z. Huang, S.-Y. Luo, M.-H. Zong, W.-Y. Lou, Multi-functional magnetic hydrogels based on Millettia speciosa Champ residue cellulose and Chitosan: highly efficient and reusable adsorbent for Congo red and Cu2+ removal, Chem. Eng. J. 423 (2021) 130198.
[69] S.P. Sinha, Structure and bonding in highly coordinated lanthanide complexes, in: Rare Earths, Springer, 2005, pp. 69–149.
[70] M.S. Hossain, M. Shenashen, M.E. Awual, A.I. Rehan, A.I. Rasee, R. Waliullah, K. T. Kubra, M.S. Salman, M.C. Sheikh, M.N. Hasan, Benign separation, adsorption, and recovery of rare-earth Yb (III) ions with specific ligand-based composite adsorbent, Process Saf. Environ. Prot. 185 (2024) 367–374.
[71] S. Shimizu, N. Matubayasi, Temperature dependence of sorption, Langmuir 37 (37) (2021) 11008–11017.
[72] J. Li, X. Zhu, Y. Zhao, M. Yang, X. Zhang, H. Chen, Q. Liu, Highly selective recovery of lanthanum and cerium from wastewater by amidoxime-modified biochar, Sep. Purif. Technol. (2025) 133303.
[73] A.-R. Chaibou Yacouba, A.E. Oral, S. Sert, I.G. Kaptanoglu, I. Natatou, S. Yusan, S. Aytas, Removal of lanthanum and cerium from aqueous solution using chitosan-functionalized magnetite-pectin, Discov. Water 4 (1) (2024) 1.
[74] E. Farahmand, Adsorption of cerium (IV) from aqueous solutions using activated carbon developed from rice straw, Open J. Geol. 6 (03) (2016) 189.

[75] Y. El-Aryan, S. Melhi, I. Ahmed, Y.A. El-Ossaily, H. Ali, B. El-Gammal, M.A. Bedair, Exploring the adsorption potential of lanthanum (III), samarium (III), and cerium (III) from aqueous solutions utilizing activated carbon derived from date seeds, Inorg. Chem. Commun. 163 (2024) 112331.
[76] S.S. Dubey, B.S. Rao, Removal of cerium ions from aqueous solution by hydrous ferric oxide–a radiotracer study, J. Hazard. Mater. 186 (2-3) (2011) 1028–1032.
[77] M.E. Awual, M.S. Salman, M.M. Hasan, M.N. Hasan, K.T. Kubra, M.C. Sheikh, A. I. Rasee, A.I. Rehan, R. Waliullah, M.S. Hossain, Ligand imprinted composite adsorbent for effective Ni (II) ion monitoring and removal from contaminated water, J. Ind. Eng. Chem. 131 (2024) 585–592.
[78] Z. Dan, C. Ji, L. Deqian, Separation chemistry and clean technique of cerium (IV): a review, J. Rare Earths 32 (8) (2014) 681–685.
[79] S. Pansambal, R. Oza, S. Borgave, A. Chauhan, P. Bardapurkar, S. Vyas, S. Ghotekar, Bioengineered cerium oxide (CeO2) nanoparticles and their diverse applications: a review, Appl. Nanosci. 13 (9) (2023) 6067–6092.
[80] T. Montini, M. Melchionna, M. Monai, P. Fornasiero, Fundamentals and catalytic applications of CeO2-based materials, Chem. Rev. 116 (10) (2016) 5987–6041.